Dissipative solitons in normal-dispersion fiber lasers

W. H. Renninger, A. Chong, and F. W. Wise
Department of Applied Physics, Cornell University, 212 Clark Hall, Ithaca, New York 14853, USA
(Received 12 September 2007; revised manuscript received 7 November 2007; published 12 February 2008)

Mode-locked fiber lasers in which pulse shaping is based on filtering of a frequency-chirped pulse are analyzed with the cubic-quintic Ginzburg-Landau equation. An exact analytical solution produces a variety of temporal and spectral shapes, which have not been observed in any experimental setting to our knowledge. Experiments agree with the theory over a wide range of parameters. The observed pulses balance gain and loss as well as phase modulations, and thus constitute dissipative temporal solitons. The normal-dispersion fiber laser allows systematic exploration of this class of solitons.

DOI: 10.1103/PhysRevA.77.023814 PACS number(s): 42.65.Tg, 42.55.Wd, 42.65.Re, 42.65.Sf

I. INTRODUCTION

Stable, localized structures (wave fronts or pulses, for example), known as dissipative solitons, can occur in a variety of physical, chemical, and biological systems [1]. Although interest in dissipative solitons has been growing in the past decade, experimental realizations of systems that support dissipative solitons are quite rare. Notable examples include the observation of spatial and temporal solitons in semiconductor optical amplifiers [2,3]. Nonlinear optics is well suited to the study of temporal solitons, but until recently optical soliton research has focused primarily on conservative solitons. In contrast to these more familiar conservative solitons that exist in nonlinear media without energy flow, gain and loss play an essential role in the formation of dissipative solitons.

The Ginzburg-Landau equation is a powerful model for many of the systems listed above. Specifically, the complex cubic Ginzburg-Landau equation (CGLE, sometimes referred to as the "master equation") is frequently used to model mode-locked lasers [4]. An analytical solution in the form of a frequency-chirped hyperbolic-secant temporal profile is known for this equation [5]. The solution has codimension zero (i.e., no relations among the system parameters are required), and this facilitates quantitative comparison of theory and experiment. The solution does not depend on position in the cavity (or along a fiber for single-pass propagation), so it strictly applies only to situations in which the pulse does not evolve appreciably. The characteristic length scales over which a pulse appreciably changes shape due to dispersive or nonlinear phase accumulations can be much shorter than the cavity length in femtosecond fiber lasers, in which case the pulse will generally breathe in the time and/or frequency domain. The static solution of the Ginzburg-Landau equation then represents some average of the pulse shape over a cavity round trip.

Recently, Chong *et al.* demonstrated a new kind of femtosecond fiber laser, in which pulse shaping is based on the spectral filtering of a highly chirped pulse in the cavity [6]. These lasers depend strongly on dissipative processes (linear gain and loss, and nonlinear saturable absorption, in addition to spectral filtering) as well as phase modulations, to shape the pulse. No anomalous group velocity dispersion (GVD) is required in the cavity, so this kind of laser is referred to as an all-normal-dispersion (ANDI) fiber laser. The absence of a dispersion map is expected to reduce breathing of the pulses. Together with the importance of the dissipative processes, this makes the ANDI laser attractive as a physical realization of the Ginzburg-Landau equation, and in particular a medium for the systematic experimental investigation of dissipative solitons. In addition to the scientific interest in understanding nonlinear pulse propagation in the ANDI laser, substantial motivation arises from its potential benefits as a scientific tool. The elimination of components with anomalous GVD significantly simplifies the laser, which can be designed for a variety of output parameters, including short pulses with very high pulse energy and peak power [7] as compared to other mode-locking techniques. The development of a model incorporating all of the features of the ANDI laser is important for future research on the performance limits of this mode-locking mechanism. A notable feature of the ANDI laser is the existence of stable pulses with a wide variety of spectral and temporal shapes [8], which are predicted by numerical simulations, but are not accounted for by analytic theory. The known solutions of the CGLE fail to account for even qualitative aspects of the ANDI laser, such as the observed spectral shapes, the pulse chirp, and a multiplicity of solutions with identical energy.

Here we show that exact stationary soliton solutions of the complex cubic-quintic Ginzburg-Landau equation (CQGLE) [a quintic nonlinear term is added to the cubic equation; see Eq. (1)] accurately model the operating modes of the ANDI laser over a wide range of parameters. The solutions include long flat-topped solitons, along with a class of pulses characterized by spectra with sharp peaks at the edges and a dip in the center. These latter solutions are observed experimentally despite the fact that they are theoretically unstable. The CQGLE was used to model additive-pulse lasers with anomalous GVD, but comparison was limited to an isolated experimental point, and was fairly crude [9]. By making some assumptions about the system parameter values, Kalashnikov *et al.* recently found an approximate solution to the CQGLE, which exhibits some of the qualitative features of the ANDI laser [10]. We find that, despite the large changes per pass in a fiber laser with a filter, the CQGLE accurately models the behavior and performance of the ANDI laser. Thus, the experiments in this work represent a comprehensive and decisive demonstration of temporal dissipative solitons in fiber. The ANDI lasers seem to

provide a nearly ideal experimental environment for investigation of a broad class of temporal dissipative solitons.

II. ANALYTICAL SOLUTION

Optical pulse evolution in the presence of the electronic Kerr nonlinearity, GVD, and dissipative processes can be modeled by the complex Ginzburg-Landau equation with cubic and quintic saturable absorber terms:

$$U_z = gU + \left(\frac{1}{\Omega} - i\frac{D}{2}\right)U_{tt} + (\alpha + i\gamma)|U|^2U + \delta|U|^4U. \quad (1)$$

U is the electric field envelope, z is the propagation coordinate, t is the retarded time, D is the GVD, g is the net gain and loss, Ω is related to the filter bandwidth, α is a cubic saturable absorber term, δ is the quintic saturable absorber term, and γ refers to the cubic refractive nonlinearity of the medium.

An exact pulse solution of Eq. (1), which generalizes the Hocking and Stewartson solution [5], as exemplified by [11] is

$$U[t,z] = \sqrt{\frac{A}{\cosh(t/\tau) + B}}\, e^{-i\beta/2\,\ln[\cosh(t/\tau)+B]+i\theta z}. \quad (2)$$

A, B, τ, β, and θ are real constants. This solution has codimension one; no solutions with codimension zero have been reported. Inserting this ansatz into Eq. (1) and separately equating the real and imaginary parts produces six equations. This system of equations admits two sets of solutions: one positively chirped with a larger amplitude and $g<0$, and the other negatively chirped with a larger pulse duration and $g>0$. We ignore the negatively chirped solutions because with $g>0$ they will be unstable against the continuous-wave background. The cubic saturable absorber term, α, is always positive for the positively chirped solutions. For fixed energy, shorter pulses experience less loss and are favored in the laser, so the pulse duration decreases until dispersive limitations are reached. With the net gain parameter g negative, these pulses are stable against the continuous-wave background.

To examine trends in the solutions, we solved for A, τ, β, θ, g, and α. Ideally, we would like to know how each of the pulse parameters varies with changes to the system parameters. Because the solution has codimension one, we must have a constraint on one of the parameters; we chose α. The energy of the pulse is calculated as the integral over time of the intensity profile. In experiments we are unable to directly adjust the net gain parameter, and instead we vary the saturation energy of the gain by adjusting the pump power. However, it is reasonable to assume that we have direct experimental control of the pulse energy [4]. This allows us to solve additionally for g, while keeping B a free parameter that we use to classify the different pulse shapes. The resulting expressions are

$$\alpha = \frac{\gamma(3\Delta + 4)}{D\Omega},$$

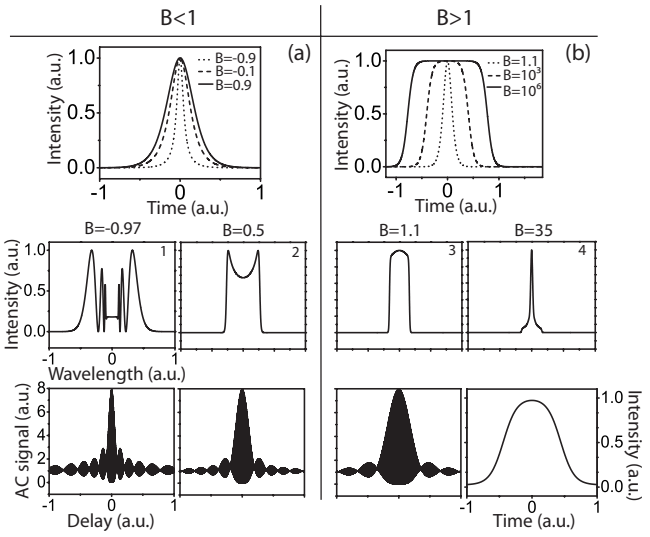

FIG. 1. Pulse solutions categorized by the value of B. Top row: temporal profiles. Middle row: representative spectral shapes for the indicated values of B. Bottom row: corresponding autocorrelations of the respective dechirped analytical solutions. The intensity profile is shown for $B=35$.

$$A = -\frac{2(B^2-1)\gamma(\Delta+2)}{BD\delta\Omega},$$

$$\tau^2 = -\frac{B^2\delta[D^2(\Delta-8)\Omega^2 + 12(\Delta-4)]}{24(B^2-1)\gamma^2\Omega(D^2\Omega^2+4)},$$

$$\beta = \frac{\Delta-4}{D\Omega},$$

$$g = -\frac{6(B^2-1)\gamma^2(D^2\Omega^2+4)[-8(\Delta-4)/D^2\Omega^2 - \Delta + 6]}{B^2\delta[D^2(\Delta-8)\Omega^2 + 12(\Delta-4)]},$$

$$\theta = -\frac{2(B^2-1)\gamma^2(\Delta+2)}{B^2D\delta\Omega},$$

$$\Delta = \sqrt{3D^2\Omega^2 + 16}. \quad (3)$$

A wide variety of pulse shapes are possible as the parameters are varied (Fig. 1). We find distinctly different solutions depending on the sign of the quintic nonlinear absorption coefficient δ. For $\delta>0$, increasing the energy produces steep-sided spectra with a dip in the middle [Fig. 1(a)]. For $\delta<0$, increasing the energy produces narrower spectra and longer, flatter pulses in the time domain [Fig. 1(b)]. These have previously been identified as "flat-topped solutions" [9]. For $B\leq -1$, no solutions exist as Eq. (2) diverges. Solutions also do not exist for $B=0$ and $B=1$, where the pulse duration goes to zero and diverges, respectively. As the energy approaches a maximum at $B=-1$ [Fig. 2(a)], the spectra exhibit deep fringes [Fig. 1(a)]. The full width at half maximum (FWHM) pulse duration is plotted in Fig. 2(b). In general, the solutions are highly chirped. In anticipation of comparing the theoretical and experimental pulse shapes, the

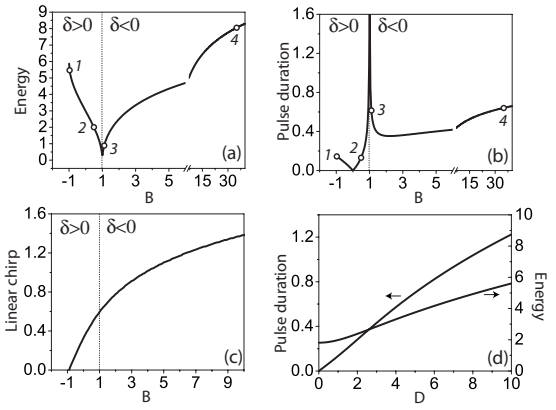

FIG. 2. (a) Energy, (b) pulse duration, and (c) chirp (normalized to that of the pulse with $B=-0.9$) plotted vs B. In (d) pulse duration and energy are plotted vs GVD parameter D. Dotted lines separate the two classes of solutions. Italicized numbers correspond to solutions shown in Fig. 1. Notice the break in the x axes in (a) and (b).

analytic solutions were numerically dechirped by impressing on them the quadratic spectral phase (corresponding to a linear dispersive delay) that minimizes the pulse duration. Then the autocorrelations of the dechirped pulses were generated (bottom row of Fig. 1). The magnitude of the required chirp is taken as the linear component of the pulse chirp. With increasing B, this chirp increases [Fig. 2(c)]. The pulse with $B=35$ can be measured directly, and we show the theoretical intensity profile instead of the autocorrelation. Variation of the pulse parameters with the cavity GVD allows comparison to other models of mode-locked lasers as well as to experiments. As is the case with the cubic master equation, the minimum pulse duration occurs at zero GVD [Fig. 2(d)] [4]. Larger pulse energies are accessible at larger normal GVD [Fig. 2(d)], as was found in numerical simulations of lasers with self-similar pulse propagation [12].

The stability of solitary wave solutions to nonlinear systems is crucial to their experimental observation. The stability of pulse solutions to the CQGLE has been studied numerically [13], for $\delta<0$. The numerical solutions are stable for a large region of parameter space, but the analytic solution of Eq. (1) is stable at only one point [corresponding to a long flat-top pulse, as in Fig. 1(b)]. The analytical solution is unstable against collapse for $\delta>0$, and as a result it has been left unexplored. Remarkably, solutions with both $\delta>0$ and $\delta<0$ are stable in the ANDI laser. This will be described in detail below, and candidate mechanisms for the stabilization will be discussed.

III. EXPERIMENTAL RESULTS

The ANDI fiber oscillator is shown schematically in Fig. 3. We use a Yb-doped gain fiber, which emits at a wavelength of 1 μm. A long (3–20 m) segment of single-mode fiber precedes the gain fiber, and a short (1 m) segment follows it in a unidirectional ring cavity. All components of the laser have normal GVD. The wave plates and polarizing beam splitter convert nonlinear polarization evolution into

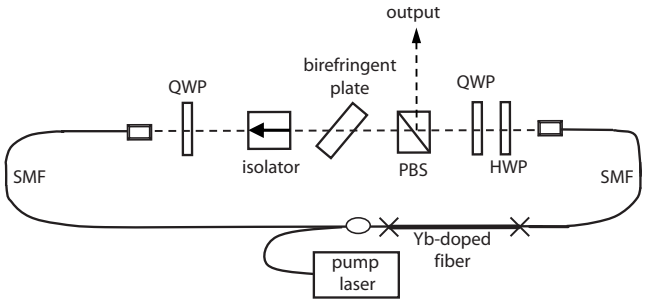

FIG. 3. Schematic of the ANDI fiber laser: QWP, quarter-wave plate; HWP, half-wave plate; PBS, polarizing beam splitter; WDM, wavelength-division multiplexer.

amplitude modulation to implement the saturable absorber. The birefringent plate surrounded by polarizers acts as an adjustable spectral filter with a sinusoidal transmission curve. We experimentally access different operating states of the laser via adjustments to the wave plates, the pump power, and the cavity length. These adjustments effectively vary the cubic and quintic saturable absorber terms, the pulse energy, and the GVD, respectively. We verified that each state presented here has only one pulse in the cavity.

The overall behavior of the laser is summarized in Fig. 4. The measured power spectra exhibit the features of the theoretical spectra in Fig. 1, which is remarkable considering the complicated spectral shapes. In fairness, the spectra in Fig. 1 are plotted with $\beta=10$, a factor of 7 from the theoretical value; this is typical of the overall quantitative agreement to the CQGLE. The spectral shapes can be tuned continuously by adjusting the pump power. For example, by increasing the pump power we can tune from $B=-0.1$ to $B=-0.97$, from $B=0.9$ to $B=0.1$, or from $B=1.1$ to $B>35$. The range in which the solution lies is determined by the saturable absorber, which is controlled by the wave plates. We infer a value of B by fitting the theoretical pulse shape to each experimental condition. Having obtained a value of B for each experimental condition, we then proceed to compare the remaining pulse parameters to the trends of Fig. 2. The dechirped autocorrelations, corresponding to the top row of Fig. 4, agree quite well with the calculated versions (bottom row of Fig. 1). The experimental chirp values increase monotonically (from 0.084 to >10 ps^2) from left to right, as pre-

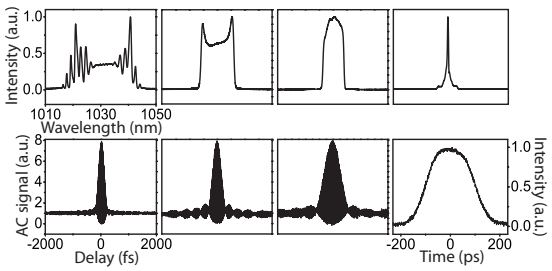

FIG. 4. Top row: representative experimental spectra corresponding to the theoretical pulses of Fig. 1. Bottom row: autocorrelation data for the corresponding dechirped pulses. The rightmost pulse is the corresponding output intensity profile.

dicted [Fig. 2(c)]. In general, pulses with $B \gg 1$ have chirp >1 ps^2, while those with $B<1$ have chirp <1 ps^2. The dechirped pulse duration also increases from left to right (from 125 fs), as theoretically predicted. Finally, the measured energies of the pulses shown in Fig. 4 also follow the theoretical trend of Fig. 2(a) with 4, 3, 2, and 8 nJ from left to right. The largest-energy single-pulsing solutions we have found correspond to the sharply peaked spectra of Fig. 1(a). For $B \approx -1$ the pulse energy reaches ~ 20 nJ [7]. Further increase of the pump power results in the loss of mode locking followed by the generation of multiple pulses.

IV. NUMERICAL SIMULATIONS

Numerical simulations of the experimental setup were also performed. Each segment of the laser is modeled by the appropriate terms of the Ginzburg-Landau equation, and coupled equations are solved for the orthogonal polarization states of light in birefringent fiber. The initial field is white noise. The stable solutions from the simulations exhibit all of the qualitative spectral features seen in Figs. 1 and 4. The simulations confirm the trends described above, and increase the quantitative agreement with experiments. In addition, some insight into the pulse evolution is obtained. The sign of the quintic nonlinear coefficient δ can be extracted from the simulations, and the results confirm the expectations above. For solutions with $B>1$, the spectral bandwidth is much less than the filter bandwidth, so there is little spectral and temporal breathing of the pulse. When $B<1$ we see that the spectral bandwidth approaches the filter bandwidth, and the temporal breathing ratio increases from 1 to the range 2–4. In that situation, the analytical solution of the CQGLE is some average of the pulse as it traverses the cavity, so the excellent agreement between the analytical solutions with $B<1$ and experiment is particularly interesting. A systematic description of the numerical simulations will be reported elsewhere.

V. SUMMARY

In summary, with $B>1$ (where $\delta<0$ is required), stable solutions to the CQGLE exist. The ANDI laser generates pulses that exhibit the characteristics of the exact analytical solution to the CQGLE. In the laser, these pulses do not breathe and so can be well modeled by the distributed CQGLE. With $B<1$ (where $\delta>0$ is required), only unstable analytical solutions to the CQGLE exist. These solutions are stabilized by the ANDI laser, as evidenced by the experiments and numerical simulations. More work will be required to prove why the solutions with $B<1$ are stable in experiments. However, several plausible mechanisms can be identified: (i) gain saturation, which is lacking from the model, is known to stabilize pulses, e.g., g from Eq. (1) can be represented as

$$g = \frac{g_0}{1 + \frac{E_{\text{pulse}}}{E_{\text{saturation}}}}; \tag{4}$$

(ii) the experimental saturable absorption may well be modeled by terms above the quintic, which could have negative coefficients; (iii) there might be breathing of the temporal pulse duration, which arises from the localized filter.

VI. CONCLUSION

The ANDI laser is modeled well by exact analytical solutions of the CQGLE, and thus constitutes a practical, robust, and dynamic test bed for studying stable solutions to the GLE and to its variants. In turn, the analysis provides theoretical explanation of a variety of spectral and temporal pulse shapes, which have not been observed previously in mode-locked lasers to our knowledge, and perhaps not in any experimental setting. These experiments represent a comprehensive and decisive demonstration of temporal dissipative solitons in fiber. This analysis can be readily adapted toward optimizing the performance of normal-dispersion fiber lasers. We hope that this class of lasers will stimulate further research into the static and breathing solutions of the Ginzburg-Landau equation and its variants.

ACKNOWLEDGMENTS

Portions of this work were supported by the National Science Foundation (Grants No. ECS-0500956 and No. PHY-0653482) and the National Institutes of Health (Grant No. EB002019). The authors thank N. Akhmediev, F. Lederer, N. Kutz, and B. Malomed for stimulating discussions.

[1] *Dissipative Solitons*, edited by N. Akhmediev and A. Ankiewics (Springer, Berlin, 2005).
[2] E. A. Ultanir, G. I. Stegeman, D. Michaelis, C. H. Lange, and F. Lederer, Phys. Rev. Lett. **90**, 253903 (2003).
[3] Z. Bakonyi, D. Michaelis, U. Peschel, G. Onishchukov, and F. Lederer, J. Opt. Soc. Am. B **19**, 487 (2002).
[4] H. A. Haus, J. G. Fujimoto, and E. P. Ippen, J. Opt. Soc. Am. B **8**, 2068 (1991).
[5] L. Hocking and K. Stewartson, Proc. R. Soc. London, Ser. A **326**, 289 (1972).
[6] A. Chong, J. Buckley, W. Renninger, and F. Wise, Opt. Express **14**, 10095 (2006).
[7] A. Chong, W. H. Renninger, and F. W. Wise, Opt. Lett. **32**, 2408 (2007).
[8] A. Chong, W. H. Renninger, and F. W. Wise, J. Opt. Soc. Am. B **25**, 140 (2008).
[9] F. I. Khatri, J. D. Moores, G. Lenz, and H. A. Haus, Opt. Commun. **114**, 447 (1995).
[10] V. L. Kalashnikov, E. Podivilov, A. Chernykh, and A. Apolonski, Appl. Phys. B: Lasers Opt. **83**, 503 (2006).
[11] W. van Saarloos and P. C. Hohenberg, Physica D **56**, 303 (1992).
[12] F. O. Ilday, J. R. Buckley, W. G. Clark, and F. W. Wise, Phys. Rev. Lett. **92**, 213902 (2004).
[13] J. M. Soto-Crespo, N. N. Akhmediev, V. V. Afanasjev, and S. Wabnitz, Phys. Rev. E **55**, 4783 (1997).